IEEE Access
Multidisciplinary ⋮ Rapid Review ⋮ Open Access Journal

Received 28 January 2025, accepted 10 February 2025, date of publication 14 February 2025, date of current version 25 February 2025.

Digital Object Identifier 10.1109/ACCESS.2025.3542460

RESEARCH ARTICLE

A Metamaterial Loaded High Gain Low Profile RHCP Microstrip Antenna for X-Band Applications

MANOJ KUMAR SHRIVASTAVA[1,2], RIPUDAMAN SINGH[2], DIPTIRANJAN SAMANTARAY[3], (Member, IEEE), AZHARUDDIN KHAN[4], ANIL KUMAR GAUTAM[5], (Senior Member, IEEE), AND AMIT KUMAR SINGH[4]

[1]Department of Electronics and Communication Engineering, GLA University, Mathura, Uttar Pradesh 281406, India
[2]Department of Electronics and Communication Engineering, IIIT Guwahati, Assam 781015, India
[3]Department of Electronics and Communication Engineering, University of Delhi, New Delhi 110007, India
[4]Department of Electronics Engineering, IIT BHU Varanasi, Varanasi, Uttar Pradesh 221005, India
[5]Department of Electronics and Communication Engineering, Govind Ballabh Pant Institute of Engineering and Technology, Pauri Garhwal, Uttarakhand 246194, India

Corresponding author: Anil Kumar Gautam (gautam1575@yahoo.co.in)

ABSTRACT This paper presents the design of a right-hand circularly polarized (RHCP) microstrip antenna loaded with metamaterial to achieve high-gain performance. The metamaterial (MTM), a 5 × 5 array of unit cells with a negative refractive index, is designed on one-sided FR4 dielectric material with dimensions $0.79\lambda_0 \times 0.79\lambda_0 \times 0.023\lambda_0$, where λ_0 is the free-space wavelength at 8.76 GHz. Both the antenna and the unit cells are designed on an FR4 substrate with a loss tangent of 0.02 and relative permittivity of 4.4. The antenna and MTM maintain the same area, with an air gap of 1 mm between them. The overall structure achieves a gain of 8.1 dBic at 9.5 GHz with stacking, compared to 4.4 dBic without the MTM stacking. The measured bandwidth of the proposed antenna is 1.98 GHz (8.76-10.74 GHz), which falls within the lower X-band, making it suitable for both military and maritime radar applications.

INDEX TERMS Microstrip antenna, RHCP, stacking, circuit analysis, metamaterial.

I. INTRODUCTION

In recent years, there has been a significant increase in research aimed at integrating metamaterials into microstrip antennas. This integration seeks to enhance key parameters such as gain, bandwidth, and directivity, thereby improving overall radiation performance. By leveraging the unique refractive index properties of metamaterials, which can range from near-zero to negative values, researchers have successfully engineered microstrip antennas to efficiently transmit electromagnetic waves within specific frequency bands in a desired direction, resulting in increased antenna gain [1]. This is achieved by leveraging the phenomenon of a negative refractive index, which causes waves to converge at a focal point along the axial direction, similar to how a convex lens focuses a light beam. By engineering the properties of the metasurface (MS), researchers can precisely customize the focal point and manipulate the radiation pattern of the microstrip antenna. This enables significant improvements in radiation characteristics, creating new opportunities for their use in various communication and sensing applications. Due to this distinctive feature, researchers have integrated metasurfaces (MS) into microstrip antennas to achieve various objectives, including enhancing antenna gain, improving MIMO isolation, reducing radar cross-section, enabling electromagnetic cloaking, and serving as microwave-absorbing materials [1], [2], [3], [4], [5], [6]. In [7], a zero-refractive-index metasurface was proposed to enhance the gain and bandwidth of a microstrip antenna designed for 5G base stations. In [8], the applicability of metasurfaces (MS) as electromagnetic cloaks has been discussed, while [9] implemented a transmission line approach to achieve cloaking

The associate editor coordinating the review of this manuscript and approving it for publication was Li Yang.

using an inductor-capacitor setup connected to a microwave system. Similarly, [10] introduced a MIMO antenna based on MS with a quasi-omnidirectional radiation pattern, designed to achieve high isolation and enhanced gain. For applications involving higher frequencies, particularly those exceeding 10 GHz, the use of circularly polarized antennas becomes essential. In this context, [11] has proposed a circularly polarized antenna that operates within an ultra-wideband frequency range of 7.55 to 20.75 GHz and exhibits high gain.

In this paper, we present a compact right-hand circularly polarized (RHCP) microstrip antenna loaded with a metamaterial (MTM) exhibiting a negative refractive index. The MTM consists of a 5 × 5 array of unit cells positioned above the radiating patch to enhance both gain and bandwidth.

II. DESIGN OF THE METAMATERIAL LOADED ANTENNA

To initiate the design of a metamaterial-loaded RHCP antenna in X-band applications, a structured approach has been followed. First, an appropriate antenna structure has been selected, such as a patch or microstrip antenna, optimized for the X-band (8-12 GHz) range. Next, a metamaterial unit cell was designed, and key properties-such as permeability, permittivity, refractive index, and impedance were analyzed to ensure the unit cell functions as a metamaterial. Common structures, such as split-ring resonators (SRRs) or electrical-LCR resonators, are typically used because their refractive indices are either negative or near negative. This characteristic helps focus the radiated energy, thereby enhancing the gain and directivity of the antenna.

The periodic boundary conditions simulate an infinite array, while a plane wave source (Floquet Port) is used to excite the unit cell. An array of unit cell (MTM) layers is positioned as a superstrate, typically placed approximately one-quarter wavelength above the antenna. This spacing promotes constructive interference in the X-band, thereby enhancing gain and shaping the radiation pattern. Through full-wave simulations, parameters such as the unit cell size, spacing, and the distance between the metamaterial layer are optimized to maximize gain. The following sections provide a comprehensive, step-by-step overview of the antenna's design process.

A. DESIGN OF UNIT CELL

Fig. 1(a) and (b) show the top and bottom views of a unit cell's structure. The unit cell has dimensions of 5 mm × 5 mm × 0.8 mm and is etched on a single-sided FR4 material. Fig. 1 also illustrates all the optimized dimensions of the unit cell. In this design, a slot is cut at the upper left corner of the rectangular ring, which functions as a ring resonator, and a metallic rectangular strip is placed within the ring. As a result, the overall structure exhibits a negative refractive index response. The scattering parameters $|S_{11}|$ (9-10.4 GHz) and $|S_{21}|$ of the unit cell are illustrated in Fig. 1(c). In Fig. 1(d) shows Floquet port set up with master and slave boundary conditions. The design and behavior of the unit cell have been analyzed using periodic boundary conditions, which simulate an infinitely repeating array by replicating a single cell across the simulation boundaries. This setup allows for efficient modelling of the MTM without the computational demands of a full array. In this configuration, plane waves are employed as the excitation source, impinging uniformly upon the unit cell. This choice of excitation is ideal for examining far-field effects and provides insight into how the metamaterial (MTM) interacts with an incoming wave over a broad area, simulating real-world applications more accurately. The properties of the individual unit cells are examined using periodic boundary conditions, and the ANSYS HFSS tool that determine the $|S_{11}|$ and $|S_{21}|$ parameters. Iterative optimization in simulation software has been employed to fine-tune these parameters, ensuring strong resonance and high negative refractive index precisely within the 8-12 GHz range.The $|S_{11}|$ and $|S_{21}|$ parameters of the individual unit cell are examined using periodic boundary conditions and the ANSYS HFSS tool. Subsequently, the permittivity, permeability, refractive index, and impedance parameters are determined using equations (1)-(4) [12], which are based on the given scattering parameters. These equations are implemented using MATLAB code and are depicted in Fig. 2. In Fig. 2(a) and Fig. 2(b), the real and imaginary components of the permittivity and permeability parameters of the unit cell are shown. Similarly, the real and imaginary components of the impedance and refractive index parameters are shown in Fig. 2(c) and (d), respectively. The real part of the refractive index exhibits a negative value within the frequency range of 8 GHz to 12 GHz, making the unit cell suitable for use as a metamaterial within this range. Furthermore, since both the permittivity and permeability have negative real values within this frequency range, the metamaterial is classified as a double-negative (DNG) metamaterial.

$$z = \sqrt{\frac{(1+S_{11})^2 - S_{21}{}^2}{(1-S_{11})^2 - S_{21}{}^2}} \tag{1}$$

$$n = \frac{1}{kd}\cos^{-1}\frac{1}{2S_{21}}\left(1 - S_{11}{}^2 + S_{21}{}^2\right) \tag{2}$$

$$\mu_{eff} = n * z \tag{3}$$

$$\epsilon_{eff} = \frac{n}{z} \tag{4}$$

where, ϵ_{eff} = effective permittivity, μ_{eff} = effective permeability, z = impedance, and n = refractive index of unit cell.

B. DESIGN OF MICROSTRIP ANTENNA

The radiating patch consists of a rectangular element with dimensions of 14.4 mm × 3 mm, attached to a semicircular arc with two circular slots positioned on either side of the center point of the antenna structure. The circular slots have a radius of 0.7 mm and are positioned along the y-axis, with each slot located 7.2 mm from the center point (0,0) of antenna structure. The antenna is designed on an FR4 dielectric material with overall dimensions of 27 mm × 27 mm × 1.6 mm. The top and bottom views of the fabricated conventional and proposed antenna prototypes,

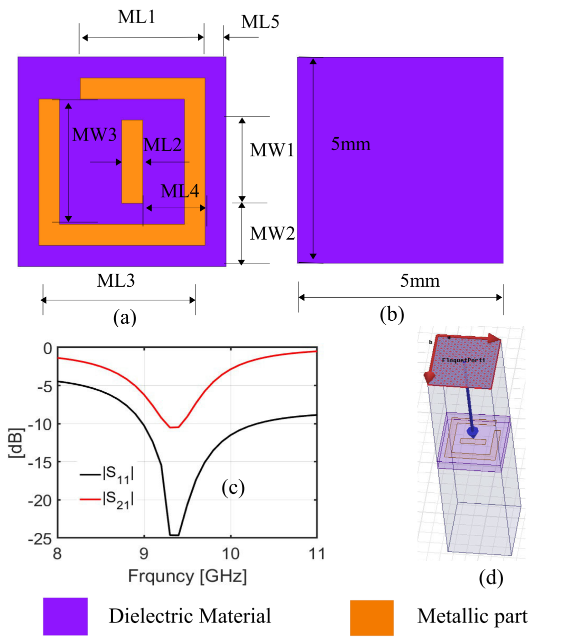

FIGURE 1. The unit cell design of MTM (a) Top view of the unit cell (b) Bottom view of the unit cell (c) $|S_{11}|$ and $|S_{21}|$ response of unit cell (d) 3D view of the simulated unit cell. (ML1 = 2.5 mm, ML2 = 0.5 mm, ML3 = 4 mm, ML4 = 1.5 mm, ML5 = 0.5 mm, MW1 = 2 mm, MW2 = 1.5 mm, MW3 = 3 mm).

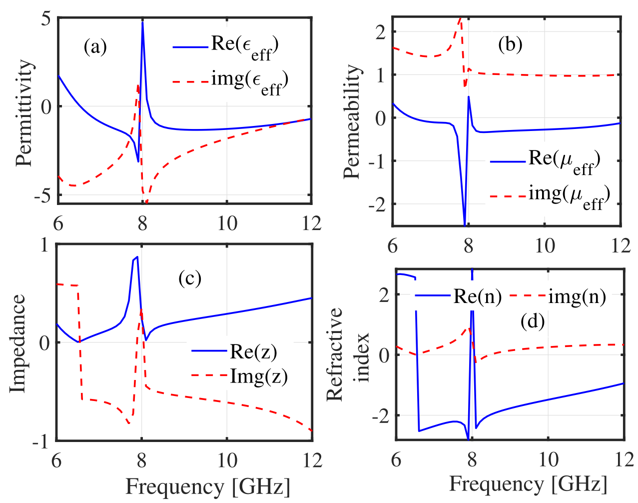

FIGURE 2. Parameters of the unit cell (a) Effective real and imaginary part of permittivity. (b) The real and imaginary part of permeability. (c) Real and imaginary part of impedance. (b) The real and imaginary parts of the refractive index.

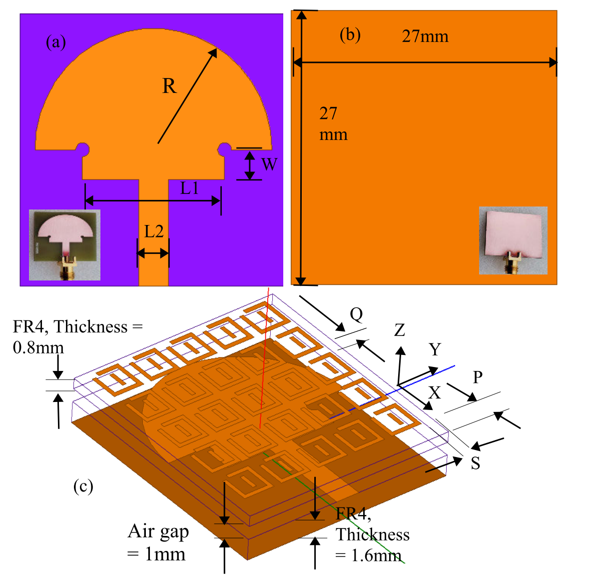

FIGURE 3. Antenna design with its dimensions (a) Top view (b) Bottom part (c) 3D view of proposed antenna prototype. (W = 3 mm, L_1 = 14.4 mm, L_2 = 3 mm, P = 2.5 mm, Q = 1 mm, R = 12 mm, S = 1.5 mm).

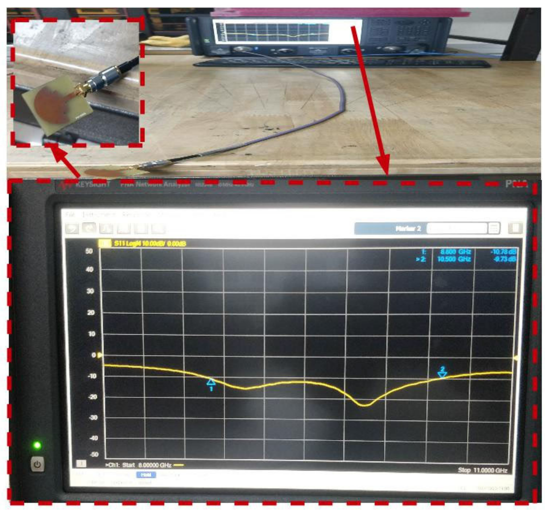

FIGURE 4. Measurement set up in the Lab of $|S_{11}|$ parameter of conventional microstrip antenna.

along with their respective dimensions, are shown in Fig. 3. Correspondingly, Fig. 4 illustrates the measurement set-up in the lab used for obtaining the $|S_{11}|$ parameters. Similarly, Fig. 5 presents the simulated and measured values of gain and $|S_{11}|$ parameters for the conventional microstrip antenna. In the simulation, the $|S_{11}|$ parameter exhibits a maximum depth of −30 dB at 9.75 GHz, with a bandwidth of 1.5 GHz (9.11-10.6 GHz), and achieves a maximum gain of 6.1 dBic at 9.56 GHz. In comparison, the measured bandwidth is 1.7 GHz (8.76-10.47 GHz), with a maximum gain of 4.4 dBic observed at 9.5 GHz.

C. DESIGN OF FINAL ANTENNA PROTOTYPE

The overall antenna structure comprises a microstrip antenna and the MTM, which includes a 5 × 5 array of unit cells. Both the individual unit cells in the MTM and the underlying planar antenna are designed according to the specifications outlined in the previous subsections. A 3D view of the proposed antenna, including its dimensions, is presented in Fig. 3(c),

TABLE 1. Components of circuit-1 and circuit-2.

Components	C_1 (fF)	L_1 (nH)	C_2 (fF)	L_2 (pH)	R_1 (Ohm)	C_3 (fF)	C_4 (fF)	L_3 (pH)	R_2 (Ohm)	C_X (fF)	C_Y (fF)
Circuit-1	61.57	4.3	857.29	444.0	109.41	428.45	126.7	362.24	167.39	49261.4	48110.3
Circuit-2	61.66	4.3	857.46	441.88	108.88	425.99	155.06	344.17	159.49	-	-

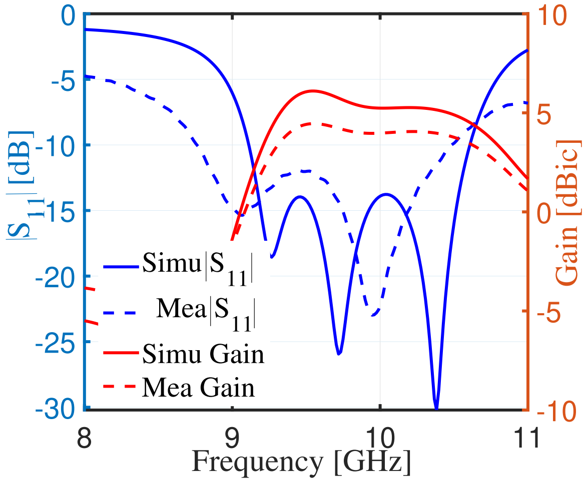

FIGURE 5. Simulated and measured $|S_{11}|$ and Gain parameters of conventional microstrip antenna. Meas. bandwidth from 8.76 GHz to 10.47 GHz, and having max. gain is 4.45 dBic at 5.53 GHz. Simu. bandwidth from 9.11 GHz to 10.6 GHz, and having max. gain is 6.1 dBic at 5.56 GHz. (antenna without meta surface).

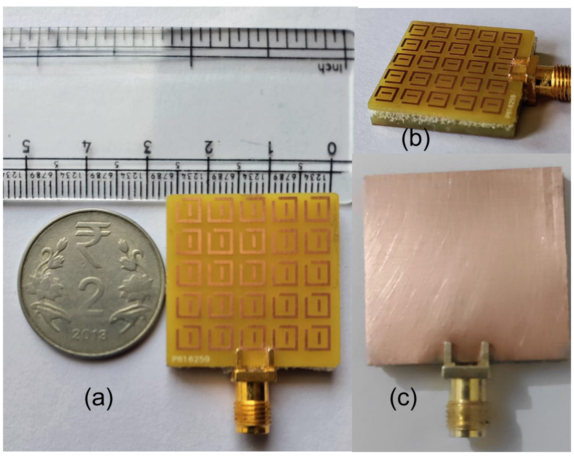

FIGURE 6. Fabricated antenna prototype (a) Top view (b) Side view (c) Back view.

while the views of the fabricated version are shown in Fig. 6. To maximize the gain, the spacing between the MTM and the planar antenna was adjusted, with an air gap of 1 mm found to provide optimal performance for the proposed antenna. As illustrated in Fig. 3(c), the distance between the rightmost column of the unit cells on the MTM and its right-side edge is 1.5 mm (denoted by S in Fig. 3(c)). Additionally, the lowermost row of the MTM is separated from its lower edge by 2.5 mm, while the uppermost row of unit cell is separated from the upper edge by 0.5 mm. After designing the proposed antenna, we developed its equivalent circuit model. The equivalent circuit of the proposed prototype is shown in Fig. 7, consisting of different combinations of L, R, and C elements. The series combination of L_1 and C_1 represent the microstrip feed line of the patch antenna. Next, the microstrip patch is modelled as a parallel combination of L_2, C_2, and R_1. Similarly, the MTM is represented by another tank circuit, modelled as parallel combination of L_3, C_4 and R_2. The 1 mm air gap between the patch and the MTM is represented by the capacitance C_3, which is sandwiched between the equivalent circuits of the antenna and the MTM. In this circuit, R_1 and R_2 represent the radiation resistances of the antenna and the MTM, respectively [13], [14]. The generation of circular polarization (CP) in this design primarily originates from the patch antenna, which consists of a semicircular element combined with a rectangular element. This configuration is responsible for producing circular polarization. Additionally, two circular slots are cut into the patch antenna to achieve the desired frequency band. In some cases, electromagnetic waves radiated by the patch antenna are converted from linear polarization (LP) to circular polarization (CP) by the MTM, or the MTM enhances the CP characteristics. These characteristics typically depend on the shape and dimensions of the MTM. However, in this design, the MTM neither creates circular polarization nor enhances CP characteristics. The CP is solely generated by the patch antenna design, while the MTM serves to converge the radiation from the antenna and enhance the gain.

The coupling capacitors C_X and C_Y represent the capacitances between adjacent unit cells along the X- and Y-axes, respectively. The capacitance resulting from the gap in the rectangular ring of the unit cell is denoted by $C_{gap} = C_4$, as shown in Fig. 7. All three of these capacitors, as shown in Fig. 8, are replaced by a single equivalent capacitor, C_4. When we simulate the S_{11} parameter of both the equivalent circuit model and the simplified equivalent circuit model, the results are all most same. This justifies that these capacitors C_X, C_Y, and C_{gap} are replaced by C_4 without any alteration in the result. After designing the simplified equivalent circuit model, we solved it using circuit theory, obtaining equations (6), (7), and (9), which represent the equivalent impedance of the first tank circuit, the coupling capacitor, and the second tank circuit. Finally, the input impedance is expressed in terms of the parallel combination of Z_1, Z_2, and Z_3, in series with C_1 andL_1, as given in equation (10). Fig. 9 presents the measured and simulated gain, along with the S_{11} parameters, including the circuit's response to S_{11}. The

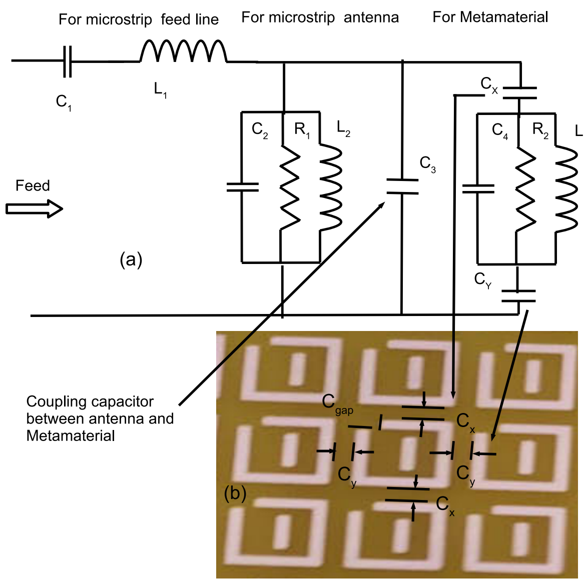

FIGURE 7. Equivalent circuit diagram of proposed prototype [Circuit-1].

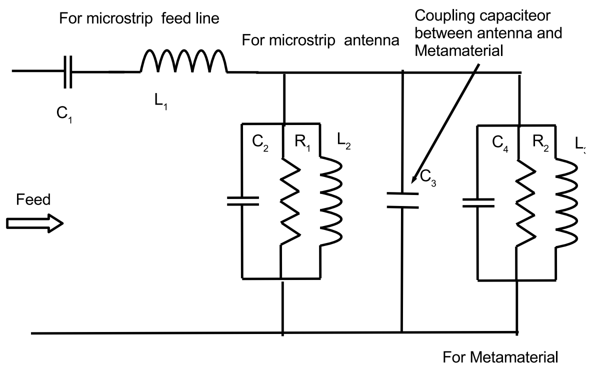

FIGURE 8. Simplified equivalent circuit diagram of proposed prototype [Circuit-2].

measured maximum gain is 8.1 dBic, while the simulated gain is 8.8 dBic at 9.5 GHz. The maximum dip in the $|S_{11}|$ parameter is observed at -24 dB in the measurements, compared to -22 dB in the simulations, with both dips occurring at 9.8 GHz. The measured bandwidth of the proposed antenna is 1.98 GHz (8.76-10.74 GHz), whereas the simulated bandwidth is 1.7 GHz (8.8-10.5 GHz). Fig. 9, also includes the S_{11} responses of the equivalent circuit model and the simplified equivalent circuit model. Both S_{11} responses are approximately the same. To facilitate a meaningful comparison, all circuit elements were kept nearly identical between the two models, except for the second tank circuit. All the components of circuit-1 and circuit-2 are shown in Table-1. Based on these S_{11} results, it can be concluded that circuit-1 can be effectively replaced by circuit-2. The second tank circuit and capacitor C_3 appear due to MTM loading in the final antenna design prototype, as shown in Fig. 8. In contrast, if we construct the equivalent circuit of a conventional antenna, no second tank circuit will be present. Thus, the input impedance of a conventional antenna does not match well with the output impedance of the measurement system. However, when a second tank circuit is added to the equivalent circuit model of the MTM-loaded antenna, it achieves better impedance matching with the output impedance of the measurement system. Therefore, the difference between the measured and simulated gain is only 0.7 dBic for the MTM-loaded antenna, whereas for the conventional antenna, the difference between the measured and simulated gain values is 1.7 dBic. All the important parameters related to the final prototype are shown in Table 2.

$$Z_1 = \frac{1}{R_1} + J\omega C_2 + \frac{1}{J\omega L_2} \tag{5}$$

$$= \frac{J\omega L_2 + J\omega C_2 (J\omega L_2)(R_1) + R_1}{R_1 (J\omega L_2)} \tag{6}$$

$$Z_2 = \frac{1}{J\omega C_3} \tag{7}$$

$$Z_3 = \frac{1}{R_2} + J\omega C_4 + \frac{1}{J\omega L_3} \tag{8}$$

$$= \frac{J\omega L_3 + J\omega C_4 (J\omega L_3)(R_2) + R_2}{R_2 (J\omega L_3)} \tag{9}$$

$$Z_{in} = J\omega L_1 + \frac{1}{J\omega C_1} + \frac{Z_1 * Z_2 * Z_3}{Z_1 + Z_2 + Z_3} \tag{10}$$

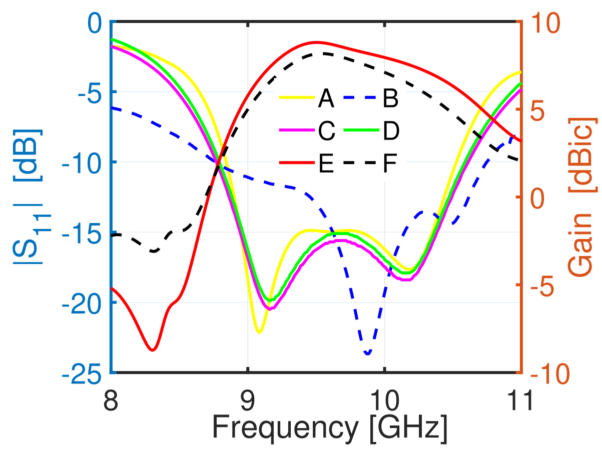

FIGURE 9. $|S_{11}|$, and gain of the designed prototype antenna. [A = Simulatd $|S_{11}|$, B = Measured $|S_{11}|$, C = $|S_{11}|$ response of Circuit-1, D = $|S_{11}|$ response of Circuit-2, E = Simulated gain of proposed antenna, and F = Measured gain of proposed antenna.]

III. DISCUSSION OF MEASURED RESULTS

The designed antenna, integrated with metamaterial, was fabricated using the photo-etching method. All relevant parameters were measured in an anechoic chamber using a KEYSIGHT N5224B PNA Microwave Network Analyzer, as depicted in Fig. 4 and Fig. 11. The simulated, analytical

TABLE 2. Some important parameters of the proposed antenna.

Results	$\|S_{11}\|$ [dB]	Bandwidth [GHz]	Max. Gain [dBic]	AR≤ $3dB$ [GHz]
Simulated	-22/-17.6	8.8-10.5	8.8	8.9-10.4
Measured	-24	8.76-10.74	8.1	9-10.4
Circuit-1	-20.1/-18.5	8.76-10.6	-	8.9-10.4
Circuit-2	-20/-18.3	8.76-10.6	-	8.9-10.4

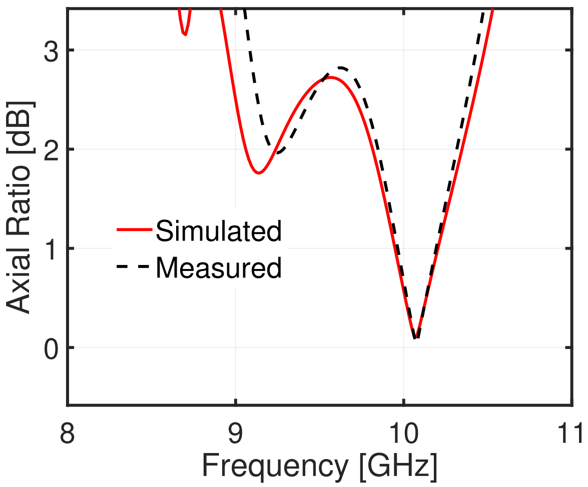

FIGURE 10. Simulated and Measured Axial ratio of designed antenna prototype.

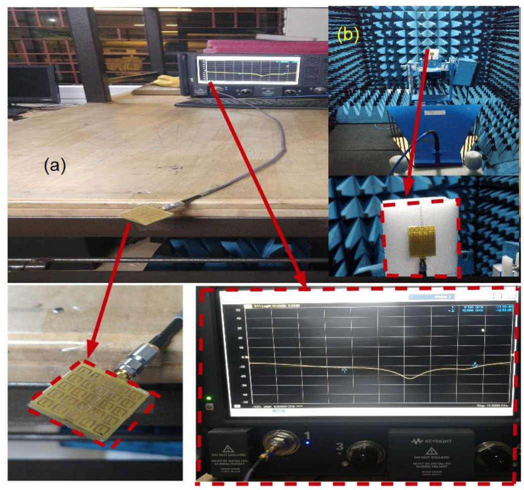

FIGURE 11. Set up in the lab (a) measuring $|S_{11}|$ parameter of the designed prototype. (b) Measurement of Radiation pattern in the lab, a calibrated Horn antenna acts as a receiver and designed prototype used as a transmitter.

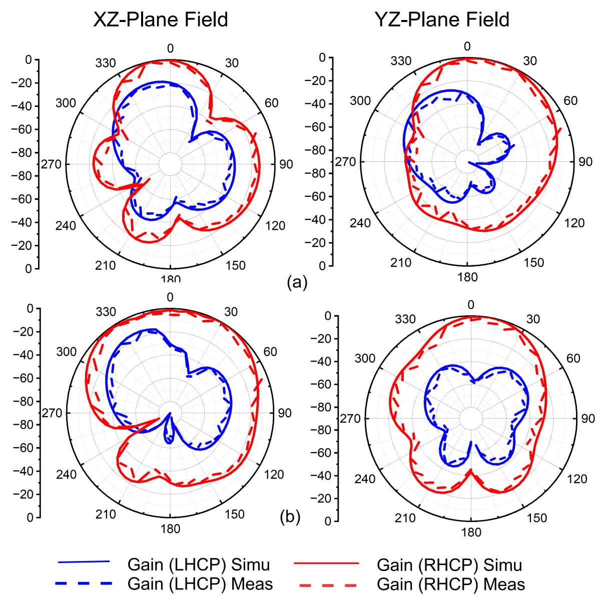

FIGURE 12. Simulated and measured 2-D radiation pattern of proposed antenna in normal dB scale at sampling frequencies (a) 9.08 GHz and (b) 10.18 GHz.

(using the equivalent circuit) models, and measured results of the MTM-based antenna have been compared in terms of axial ratio bandwidth, impedance bandwidth, and realized gain, as summarized in Table 2. Fig. 9 shows the simulated and measured values of the S_{11} and gain parameters. It also includes the S_{11} parameter obtained through circuit analysis, which was achieved using Advanced Design System (ADS) software. The maximum simulated gain is 8.8 dBic at 9.5 GHz, while the measured gain is 8.1 dBic at the same frequency.

Fig. 10 illustrates the measured and simulated values of the axial ratio (AR) bandwidths for the prototype. It is observed that the simulated and measured AR bandwidths range from 8.9 GHz to 10.48 GHz and from 9 GHz to 10.43 GHz, respectively, which is slightly narrower than the impedance bandwidth of 8.76-10.74 GHz. The measurement set-up for the proposed prototype is shown in Fig. 11. Additionally, Fig. 12 presents the 2D plots of the normalized radiation patterns (in dB) of the prototype at frequencies of 9.08 GHz and 10.18 GHz in the xz and yz planes, respectively. Notably, the difference between RHCP and LHCP is at least 15 dB, except for a few angles. The dominant radiation field is RHCP, as observed in Fig. 12. In these radiation patterns, the field exhibits maximal values within the upper half-plane of the radiation pattern for both sampling frequencies.

One of the key parameters in antenna design is radiation efficiency (R_{effi} = Gain/Directivity), which is shown in Fig. 13. The maximum simulated and measured efficiencies are found to be 93.1% and 91.2%, respectively, at a frequency

TABLE 3. Comparative study of the proposed antenna with some other high gain antennas.

Ref.	Size of Antenna (multiple of λ_0)	Bandwidth [GHz]	Gain [dBic]	Polarization
[15]	$1.16 \times 1.16 \times 0.26$	4.9-5.5	9.3	LP.
[16]	$3.6 \times 3.6 \times 0.14$	12.6-13.76	9.1	LP
[17]	$3.1 \times 3.1 \times 0.6$	55.6-69.6	18.8	LP
[18]	$2.2 \times 2.2 \times 0.6$	9.4-11.1	12	LP
[19]	$0.9 \times 0.9 \times 0.29$	9.24-11.25	7.57	LP
[20]	$0.39 \times 0.11 \times 0.0014$	0.88-0.97, 2.41-2.48, & 5.77-5.91	6	LP
[21]	$0.99 \times 0.99 \times 0.09$	2.9-4.5	9	CP
[22]	$1.54 \times 1.54 \times 0.057$	5.25-6.35	5.6	CP
This work	$0.79 \times 0.79 \times 0.023$	8.5-10.74	8.1	CP

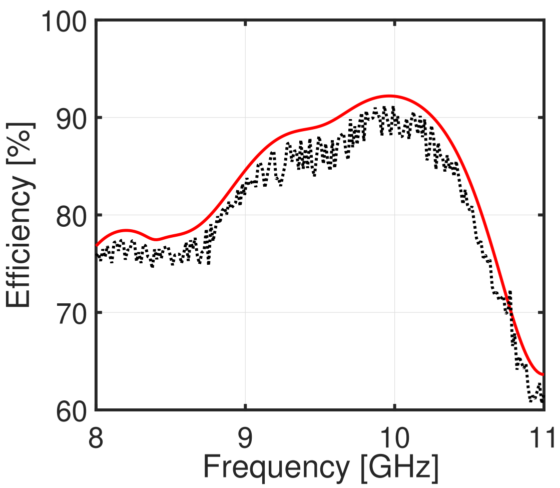

FIGURE 13. Simulated and measured radiation efficiency of proposed antenna.

of 10 GHz. Minor variations during fabrication, such as slight misalignments or deviations in unit cell dimensions, can influence the resonant behaviour of the metamaterial. These variations may impact both the gain (efficiency) and frequency response when compared to the idealized simulation results. Additionally, experimental testing in an anechoic chamber can introduce reflections or positioning inaccuracies, leading to slight variations in the measured results. Surface roughness and additional losses in the metamaterial layer or feed network may also attenuate signals more than expected, contributing to discrepancies between the measured and simulated results. A comparison of the performance between the proposed antenna and several recently reported works is presented in Table 3, based on parameters such as size, bandwidth, gain, and polarization. As shown in Table 3, the integration of a metamaterial layer as a superstrate above the antenna significantly boosts gain without necessitating a larger antenna aperture [15], [16], [17], [18], [19], [20], [21], [22]. Certainly, papers such as [15], [16], [17], [18], and [21] report higher gains than the proposed antenna, but their profile sizes are larger. There is a trade-off between the size and gain of the antenna, and in this prototype, an optimal gain has been achieved for a smaller size compared to the antennas discussed in Table 3.

However, our metamaterial-loaded design improves RHCP purity across the X-band frequency range, an area where many conventional designs face challenges. Moreover, from [15], [16], [17], [18], [19], and [20], it can be inferred that most high-gain antennas are linearly polarized and have a high profile, except for [20] (which has a lower gain). Only a few designs, such as [20] and [21], are circularly polarized; of these, [21] offers higher gain than our design but has a larger profile size. Therefore, our designed antenna is an excellent candidate for achieving high gain with a low profile

IV. CONCLUSION

A DNG MTM-loaded RHCP microstrip antenna has been designed for gain enhancement. The antenna without MTM has a bandwidth of 1.71 GHz (8.76-10.47 GHz), whereas the antenna with MTM has a bandwidth of 1.98 GHz (8.76-10.74 GHz), resulting in a fractional bandwidth of 20.3%. It is observed that the maximum gain with MTM stacking is 8.1 dBic, whereas the maximum gain without MTM stacking is 4.45 dBic. The measured 3 dB axial ratio bandwidth ranges from 9 to 10.4 GHz, which is slightly less than the required bandwidth of 8.76 to 10.74 GHz. The use of MTM results in a gain enhancement of 3.7 dBic (from 4.4 dBic to 8.1 dBic) and a bandwidth enhancement of 0.27 GHz (from 1.71 GHz to 1.98 GHz). This antenna is well-suited for radar applications in both military and maritime domains.

REFERENCES

[1] B. A. F. Esmail, S. Koziel, and S. Szczepanski, "Overview of planar antenna loading metamaterials for gain performance enhancement: The two decades of progress," *IEEE Access*, vol. 10, pp. 27381–27403, 2022.

[2] J. Yang, C. Huang, J. Song, X. Zhang, X. Xie, and X. Luo, "Metasurface-based lens for antenna gain enhancement and radar cross section reduction," *IEEE Photon. J.*, vol. 11, no. 6, pp. 1–9, Dec. 2019.

[3] D. Samantaray, S. K. Ghosh, and S. Bhattacharyya, "Modified slotted patch antenna with metasurface as superstrate for dual-band applications," *IEEE Antennas Wireless Propag. Lett.*, vol. 22, pp. 109–113, 2023.

[4] N. C. Pradhan, K. S. Subramanian, R. K. Barik, and S. Koziel, "Shielded HMSIW-based self-triplexing antenna with high isolation for WiFi/WLAN/ISM band," *IEEE Trans. Circuits Syst. II, Exp. Briefs*, vol. 70, no. 6, pp. 1941–1945, Jun. 2023.

[5] S. Sarkar and B. Gupta, "An ultrathin multiband chiral metasurface for transmission and asymmetric absorption of electromagnetic waves," *Int. J. RF Microw. Comput.-Aided Eng.*, vol. 2024, no. 1, Jan. 2024, Art. no. 2326362.

[6] B. Cai, L. Wu, X. Zhu, Z. Cheng, and Y. Cheng, "Ultra-broadband and wide-angle plasmonic light absorber based on all-dielectric gallium arsenide (GaAs) metasurface in visible and near-infrared region," *Results Phys.*, vol. 58, Mar. 2024, Art. no. 107509.

[7] K. Gulur Sadananda, M. P. Abegaonkar, and S. K. Koul, "Gain equalized shared-aperture antenna using dual-polarized ZIM for mmWave 5G base stations," *IEEE Antennas Wireless Propag. Lett.*, vol. 18, pp. 1100–1104, 2019.

[8] A. Rajput and K. V. Srivastava, "Approximated complementary cloak with diagonally homogeneous material parameters using shifted parabolic coordinate system," *IEEE Trans. Antennas Propag.*, vol. 65, no. 3, pp. 1458–1463, Mar. 2017.

[9] X. Liu, C. Li, K. Yao, X. Meng, and F. Li, "Invisibility cloaks modeled by anisotropic metamaterials based on inductor-capacitor networks," *IEEE Antennas Wireless Propag. Lett.*, vol. 8, pp. 1154–1157, 2009.

[10] P. Wang, J. Liu, G. Huang, Q. Wu, C. Zhou, and W. Wang, "Wideband gain enhancement of high-isolation and quasi-omnidirectional metamaterial MIMO antenna for vehicular radar," *IEEE Trans. Instrum. Meas.*, vol. 71, pp. 1–12, 2022.

[11] Z. Liu, Y. Liu, and S. Gong, "Gain enhanced circularly polarized antenna with RCS reduction based on metasurface," *IEEE Access*, vol. 6, pp. 46856–46862, 2018.

[12] D. R. Smith, D. C. Vier, T. Koschny, and C. M. Soukoulis, "Electromagnetic parameter retrieval from inhomogeneous metamaterials," *Phys. Rev. E, Stat. Phys. Plasmas Fluids Relat. Interdiscip. Top.*, vol. 71, no. 3, Mar. 2005, Art. no. 036617.

[13] S. B. T. Wang, A. M. Niknejad, and R. W. Brodersen, "Circuit modeling methodology for UWB omnidirectional small antennas," *IEEE J. Sel. Areas Commun.*, vol. 24, no. 4, pp. 871–877, Apr. 2006.

[14] D. Samantaray and S. Bhattacharyya, "A metasurface-backed planar low-profile dual-band monopole antenna," *J. Electromagn. Waves Appl.*, vol. 37, nos. 7–9, pp. 884–897, Jun. 2023.

[15] Y. F. Cao and X. Y. Zhang, "A wideband beam-steerable slot antenna using artificial magnetic conductors with simple structure," *IEEE Trans. Antennas Propag.*, vol. 66, no. 4, pp. 1685–1694, Apr. 2018.

[16] A. Sharma, D. Gangwar, B. Kumar Kanaujia, S. Dwari, and S. Kumar, "Design of a wideband polarisation conversion metasurface and its application for RCS reduction and gain enhancement of a circularly polarised antenna," *IET Microw., Antennas Propag.*, vol. 13, no. 9, pp. 1427–1437, Jul. 2019.

[17] A. A. Baba, R. M. Hashmi, K. P. Esselle, J. G. Marin, and J. Hesselbarth, "Broadband partially reflecting superstrate-based antenna for 60 GHz applications," *IEEE Trans. Antennas Propag.*, vol. 67, no. 7, pp. 4854–4859, Jul. 2019.

[18] Y. Zheng, J. Gao, Y. Zhou, X. Cao, H. Yang, S. Li, and T. Li, "Wideband gain enhancement and RCS reduction of Fabry–Pérot resonator antenna with chessboard arranged metamaterial superstrate," *IEEE Trans. Antennas Propag.*, vol. 66, no. 2, pp. 590–599, Feb. 2018.

[19] D. Samantaray and S. Bhattacharyya, "A gain-enhanced slotted patch antenna using metasurface as superstrate configuration," *IEEE Trans. Antennas Propag.*, vol. 68, no. 9, pp. 6548–6556, Sep. 2020.

[20] M. Abdelkarim, A. Gharsallah, and R. Faouel, "Analysis and design of a high gain multiband antenna based on metamaterials for RFID applications," *Int. J. RF Microw. Comput.-Aided Eng.*, vol. 2024, pp. 1–20, Mar. 2024.

[21] C. Cao and C. Guo, "A wideband high-gain LHCP/RHCP patch antenna based on mirror feed method," *IEEE Antennas Wireless Propag. Lett.*, vol. 21, pp. 2317–2321, 2022.

[22] Q. Zheng, C. Guo, J. Ding, and G. A. E. Vandenbosch, "A broadband low-RCS metasurface for CP patch antennas," *IEEE Trans. Antennas Propag.*, vol. 69, no. 6, pp. 3529–3534, Jun. 2021.

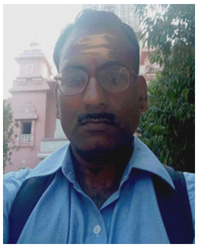

MANOJ KUMAR SHRIVASTAVA was born in East Champaran, Bihar, India, in 1974. He received the B.Tech. degree in electronics engineering from the Institute of Engineering, Pulchowk Campus, Tribhuvan University, Nepal, in 2002, and the master's degree in electronics engineering from IIT (BHU) Varanasi, Varanasi, India, in 2012. He is currently pursuing the Ph.D. degree with Indian Institute of Information Technology (IIIT) Guwahati, India. His research interests include ultra-wideband (UWB) antennas, circularly polarized metamaterial-based antennas, and cloaking using metamaterials.

RIPUDAMAN SINGH received the B.E. degree (Hons.) in electronics and communication engineering from the University of Rajasthan, Jaipur, India, in 2009, and the M.Tech. and Ph.D. degrees in electronics and electrical engineering from Indian Institute of Technology Guwahati, Guwahati, India, in 2012 and 2018, respectively.

He is currently an Assistant Professor with the Department of Electronics and Communication Engineering, Indian Institute of Information Technology Guwahati. From May 2020 to December 2020, he was a Postdoctoral Fellow with the Electrical and Computer Engineering Department, National University of Singapore, Singapore. His research interests include wireless sensor networks, distributed algorithms, antenna design, and performance modeling of communication systems.

DIPTIRANJAN SAMANTARAY (Member, IEEE) received the B.Tech. degree in electronics and telecommunication engineering from the Biju Patnaik University of Technology, Rourkela, India, in 2009, the M.Tech. degree in electronics and communication engineering from Indian Institute of Technology Kharagpur, India, in 2015, and the Ph.D. degree in microwave engineering from Indian Institute of Technology (Banaras Hindu University), Varanasi, India, in 2022. Currently, he is an Assistant Professor with the Department of Electronics and Communication Engineering, Faculty of Technology, University of Delhi. His research interests include electromagnetic, antennas, and metamaterials. In his teaching and research experience, he has authored or co-authored many technical papers in international journals and conference proceedings. He served as the Founding Treasurer for the IEEE Photonics Society Student Branch Chapter and the Chairperson of the IEEE MTT-S Student Branch Chapter, IIT (BHU) Varanasi.

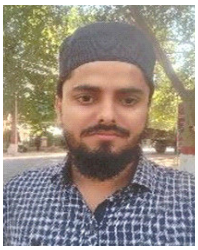

AZHARUDDIN KHAN received the Ph.D. degree from IIT (BHU) Varanasi, Varanasi, India, in 2023. Currently, he is a RF Design Engineer. He has published and co-authored over 15 journal articles and conference papers. His research interests include the design of patch antennas for biomedical application, RFID antennas, SIW antennas, specific absorption rate reduction techniques, and metamaterials.

ANIL KUMAR GAUTAM (Senior Member, IEEE) received the B.E. degree in electronics and communication engineering from the BT Kumaon Institute of Technology, Almora, India, in 1999, and the Ph.D. degree in electronic engineering from Indian Institute of Technology (BHU) Varanasi, India, in 2007.

In 2000, he joined the Department of Electronics and Communication Engineering, Govind Ballabh Pant Institute of Engineering and Technology, Pauri Garhwal, India, as an Assistant Professor and appointed as Associate Professor, in 2009. He was a Professor and the Dean of the School of Information and Communication Technology, Gautam Buddha University, Greater Noida, India, from 2016 to 2018. He was the Dean (Academic) of the School of ICT, the Head of the Department, a Registrar of the Govind Ballabh Pant Institute of Engineering and Technology, Pauri Garhwal, India, in 2016. He is currently a Professor with the Department of Electronics and Communication Engineering, Govind Ballabh Pant Institute of Engineering and Technology. He has delivered many expert talks in FDP, workshops, and STCs. He has supervised his 33 M.Tech. and eight Ph.D. theses and currently supervising his one Ph.D. theses in microstrip antenna. He has authored or co-authored more than 125 SCI research articles published in the refereed international journals, such as IEEE Transactions on Antenna and Propagation, IEEE Antenna and Wave Propagation Letters, and *Microwave and Optical Technology Letters* (Springer). He has authored 13 books in electronics engineering, with a focus on digital electronics, antenna, and microwave engineering. His current research interests include design and modelling of active microstrip antenna, microstrip antennas with defected ground structure, ultrawide bandwidth antennas, reconfigurable antennas, reconfiguration antenna array, and circular polarized antenna.

Dr. Gautam was the Chairman of the Board of Study, School of Information and Communication Technology, and a member of the Board of Management and Academic Council, Gautam Buddha University. He is also an Active Member of the Board of Study, Academic Council, and many other academic committees of GBPEC, Pauri Garhwal. He is also a member of the BOS, Hemwati Nandan Bahuguna Garhwal University, Srinagar, India, and Uttarakhand Technical University, Dehradun, India. He was a Nodal Officer, TSP, and SCSP Grants by the Government of Uttarakhand and executed several projects under these grants. He is a member of Editorial Board of the *International Journal of RF and Microwave Computer-Aided Engineering*. He is also in reviewers' panel of IEEE Transactions on Antenna and Propagation, IEEE Antenna and Wave Propagation Letters, *IET Microwaves, Antennas & Propagation*, *Wireless Personal Communications* (Springer), the *International Journal of Electronics*, the *International Journal of Microwave and Wireless Technologies*, and the *International Journal of Antenna and Propagation*. He is a member various other technical societies also. He was a recipient Education Leadership Awards, in 2018, awarded by Dewang Mehta National Education Awards, India. His paper titled "Tapered Fed Compact UWB MIMO-Diversity Antenna With Dual Band-Notched characteristics has awarded First prize of "Governor's Award 2019" for Best Research Paper by Governor, State of Uttarakhand.

AMIT KUMAR SINGH received the Ph.D. degree from IIT (BHU), Varanasi, in 2010. He has been an Associate Professor with the Electronics Engineering Department, IIT (BHU) Varanasi, since 2012. He has published and co-authored over 70 journal articles and conference papers. His research interests include the design of millimetre frequency antennas, feeds for parabolic reflectors, dielectric resonator antennas, microstrip antennas, EBG, artificial magnetic conductors, soft and hard surfaces, antennas for RFIDs, phased array antennas, and computer aided design for antennas.